Nature of order-disorder charge-density-wave phase transition in kagome metal RbV_3Sb_5

Shichang Yao,[1,*] Chongze Wang,[1] Zhenzhen Feng,[1] Bing Wang,[1] Yu Jia,[1,2,3] Zhenyu Zhang,[4,†] and J. Cho[1,‡]

[1]*Joint Center for Theoretical Physics, School of Physics and Electronics, Henan University, Kaifeng 475004, People's Republic of China*

[2]*Institute of Quantum Materials and Physics, Henan Academy of Sciences, Zhengzhou 450046, China*

[3]*Key Laboratory for Special Functional Materials of the Ministry of Education, Henan University, Kaifeng 475004, China*

[4]*International Center for Quantum Design of Functional Materials (ICQD), and Hefei National Laboratory, University of Science and Technology of China, Hefei 230026, China*

(Received 29 November 2023; accepted 11 June 2024; published 20 June 2024)

Using first-principles density-functional theory calculations and free energy analysis, we demonstrate that for RbV_3Sb_5, the long-range $2\times2\times2$ charge density wave (CDW) is condensed from the disordered 2×2 charge orders at T_{CDW}, indicating an order-disorder nature of CDW phase transition. It is revealed that the dynamic fluctuations of four degenerate 2×2 charge orders exist above T_{CDW}, giving rise to a configurational entropy. Our free energy analysis predicts the first-order transition with a release of entropy at $T_{CDW} \approx 95$ K, consistent with the measured specific heat data showing the presence of a sharp peak across the phase transition. Furthermore, we identify that the CDW fluctuations above T_{CDW} occur through a thermal reaction with the concerted V-V bond breakages and formations of V trimers and hexamers, corroborated by the experimental evidence of strong CDW fluctuations extending to higher than $\sim1.7 \times T_{CDW}$. The present results not only shed light on the nature of the first-order, order-disorder CDW phase transition in AV_3Sb_5 but also have broader implications for understanding the disorder-induced collapse of long-range CDW order in other kagome metals such as ScV_6Sn_6 and FeGe.

DOI: 10.1103/PhysRevMaterials.8.064002

I. INTRODUCTION

The two-dimensional (2D) kagome lattice, made of corner-sharing triangles, has attracted significant interest in condensed matter physics because it provides an ideal platform to investigate novel quantum phenomena including geometrical frustration, nontrivial topological states, and strong electron correlations [1–3]. Specifically, a family of V-based kagome metals AV_3Sb_5 (A = K, Rb, Cs) consisting of three-atom-thick Sb-V_3Sb-Sb and one-atom-thick A layers [see Fig. 1(a)] has been observed to exhibit a variety of exotic quantum states such as unconventional charge density waves (CDWs), electronic nematicity, anomalous Hall effect without long-range magnetic orders, and superconductivity [4–10]. The electronic structure of AV_3Sb_5 compounds shows the saddle points of linearly dispersive Dirac bands at three inequivalent M points of the Brillouin zone near the Fermi level E_F. Consequently, the Fermi surface nesting (FSN) of such van Hove singularities (VHSs) was proposed to be a driving mechanism of the CDW formation through an electronic instability arising from a diverged susceptibility [8,11–14]. However, other mechanisms based on phonon softening [15] arising from momentum-dependent electron-phonon coupling [16–22] or Jahn-Teller-like distortion [23] have also been proposed [24].

Earlier scanning tunneling microscopy [12,13], angle-resolved photoemission spectroscopy [8], and optical spectroscopy [14] studies proposed the FSN scenario of the saddle point-derived VHSs at the M point, which can be readily derived from the band structure of an ideal 2D kagome lattice with s orbital [11]. However, this scenario has been questionable because the Fermi surface of the pristine phase of bulk CsV_3Sb_5, obtained using density-functional theory (DFT) calculations, hardly produces a dominant peak of electronic susceptibility at the M point [23,26]. Meanwhile, although the calculated phonon spectrum of the pristine phase of AV_3Sb_5 exhibits soft modes at the M and L points with imaginary frequencies [27,28], inelastic x-ray, neutron, and Raman scattering experiments [29] have shown no evidence of the anomaly of the low energy acoustic phonon dispersion across the CDW phase transition, indicating the absence of the Kohn anomaly. Therefore, the FSN and phonon softening scenarios for the CDW phase transition in AV_3Sb_5 have conflicts between existing experimental and theoretical studies.

Meanwhile, recent diffuse scattering (DS) and inelastic x-ray scattering (IXS) experiments [30] for RbV_3Sb_5 and CsV_3Sb_5 reported that (i) the phonon fluctuations of 3D $2\times2\times2$ CDW are identified above T_{CDW} ($\sim$104 K for RbV_3Sb_5 and $\sim$94 K for CsV_3Sb_5) while they are suppressed to form a long-range $2\times2\times2$ CDW order below T_{CDW} and (ii) the intensity of the quasielastic central peak of IXS follows the DS intensity across the CDW phase transition, indicating an order-disorder type without phonon softening. Furthermore, heat capacity, electrical, and thermal transport measurements [31] of AV_3Sb_5 also demonstrated the development of short-range CDW fluctuations above T_{CDW}. Specifically, for CsV_3Sb_5, the disordered phase with

*Contact author: ysclord@gmail.com
†Contact author: zhangzy@ustc.edu.cn
‡Contact author: cho@henu.edu.cn

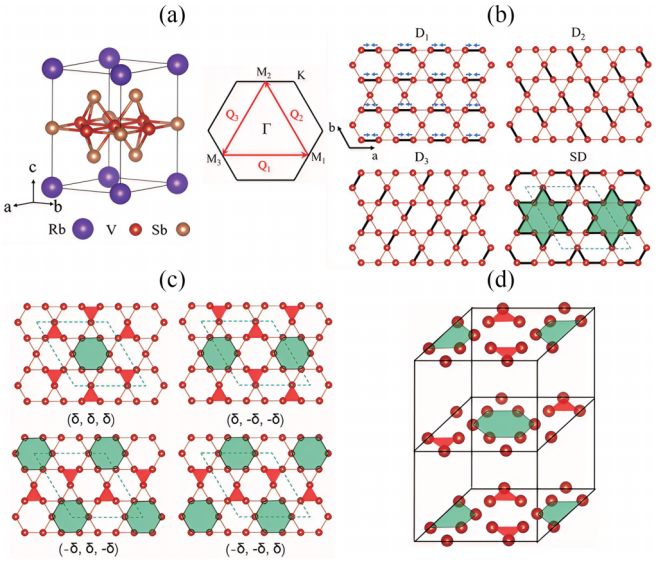

FIG. 1. (a) Crystal structure of the pristine phase of RbV_3Sb_5, together with Brillouin zone. Here, $\mathbf{Q}_1$, $\mathbf{Q}_2$, and $\mathbf{Q}_3$ represent vectors connecting different M points. The SD kagome structure composed of three one-dimensional V-dimer chains D_1, D_2, and D_3 is displayed in (b), where the arrows indicate the direction of V-atom displacements and the dashed line represents the 2×2 unit cell. The patterns of V-kagome lattice in four degenerate 2×2×1 ISD configurations are drawn in (c) and the π-shifted 2×2×2 ISD structure is drawn in (d).

CDW fluctuations extends up to ∼160 K, equivalent to $\sim 1.7 \times T_{CDW}$ [32]. This experimental evidence of the order-disorder-type CDW phase transition at T_{CDW} contrasts with the FSN and phonon softening scenarios accompanying displacive structural transformations from the pristine phase [11,18–22,33–36]. However, the nature of the observed order-disorder CDW phase transition in AV_3Sb_5 is yet to be explored.

In this Letter, we explore the atomic-scale understanding of the order-disorder CDW phase transition in RbV_3Sb_5 using first-principles DFT calculations and free energy analysis. For $T > T_{CDW}$, the disorder phase is characterized by the dynamic fluctuations between four degenerate 2×2 charge orders, which occur through a thermal reaction with the consecutive bond-breaking and bond-making processes of V trimers and hexamers. However, as temperature lowers toward T_{CDW}, such CDW fluctuations are suppressed and replaced by the long-range 2×2×2 CDW phase with a release of entropy, indicating a first-order, order-disorder CDW phase transition. By comparing the Helmholtz free energies of the order and disorder CDW phases, we predict T_{CDW} as ∼95 K, close to the experimental $T_{CDW} \approx 104$ K. Our findings provide an explanation for the recently observed order-disorder transition in the CDW phase of AV_3Sb_5 [30–32], with broader implications for such CDW phase transitions reported in other kagome metals like ScV_6Sn_6 [37–39] and FeGe [40].

II. CALCULATIONAL METHODS

Our first-principles DFT calculations were performed using the Vienna *ab initio* simulation package with the projector-augmented wave method [41–43]. For the exchange-correlation energy, we employed the generalized-gradient approximation functional of Perdew-Burke-Ernzerhof [44]. The plane wave basis was employed with a kinetic energy cutoff of 500 eV, and the k-space integration was done with 6×6×8 and 6×6×4 meshes for the 2×2×1 and 2×2×2 phases, respectively. For the electronic (phononic) density of states (DOS) calculations of the 2×2×1 and 2×2×2 phases, we used dense 18×18×24 (64×64×64) and 18×18×12 (36×36×36) k meshes, respectively, which give sufficiently converged results. All atoms were allowed to relax along the calculated forces until all the residual force components were less than 0.0001 eV/Å. The phonon dispersions were calculated using the finite displacement method implemented in the phonopy software [45,46]. The energy barrier along the transition pathway between two degenerated 2×2×1 phases is calculated using the nudged elastic band method [47,48].

III. RESULTS AND DISCUSSION

It has been well established that the CDW order of AV_3Sb_5 accompanies the lattice distortion of V kagome layer with a 2×2 periodicity, forming the so-called Star-of-David (SD) or inverse Star-of-David (ISD) structure [27]. As shown in Fig. 1(b), the SD structure is constructed by the combination of three 2×1 1D V-dimer chains D_1, D_2, and D_3 along the $\mathbf{Q}_1$, $\mathbf{Q}_2$, and $\mathbf{Q}_3$ directions, respectively. Here, if these dimerized charge bond orders D_1, D_2, and D_3 flip the directions of the displacements of V atoms, SD turns into ISD which has a periodic arrangement of V atoms in triangles and hexagons [see Fig. 1(c)]. We note that there are four translationally equivalent ISD configurations with shifting one pristine lattice constant along the $\mathbf{Q}_1$, $\mathbf{Q}_2$, and $\mathbf{Q}_3$ directions. These 2×2 SD and ISD charge orders can be stacked along the c axis to form a certain 3D CDW order [13,49,50]. There have been proposed different-type 3D CDW orders in AV_3Sb_5 [49,50], such as π-shifted ISD between neighboring kagome layers [see Fig. 1(d)] and mixed SD and ISD. For CsV_3Sb_5, x-ray diffraction studies [50] reported the observation of diverse 3D CDW phases with the 2×2×2 or 2×2×4 unit cell. The experimental observations of multiple 3D CDW phases in CsV_3Sb_5 under specific growth conditions [49] may be attributed to weak interlayer interactions, likely arising from the larger size of intercalated Cs atoms. In contrast, compelling experimental evidence [12,49] supports the presence of a single 2×2×2 CDW phase with a π-shifted ISD structure in KV_3Sb_5 and RbV_3Sb_5 [see Fig. 1(d)]. This suggests that stronger interlayer interactions in KV_3Sb_5 and RbV_3Sb_5 compared to CsV_3Sb_5 play a crucial role in determining the single 3D CDW order observed in these materials. Consequently, RbV_3Sb_5 is selected for investigating the nature of the observed [30–32] order-disorder CDW phase transition at T_{CDW}.

To determine the order-disorder CDW phase transition between π-shifted ISD (hereafter, designated π-ISD) and disordered ISD (designated d-ISD) in RbV_3Sb_5, we calculate their Helmholtz free energies $F = E + E_{vib} - TS$ where E_{vib} represents vibrational energy and S includes three different types of entropy such as vibrational entropy S_{vib}, electronic entropy S_{el}, and configurational entropy S_{con}. Here,

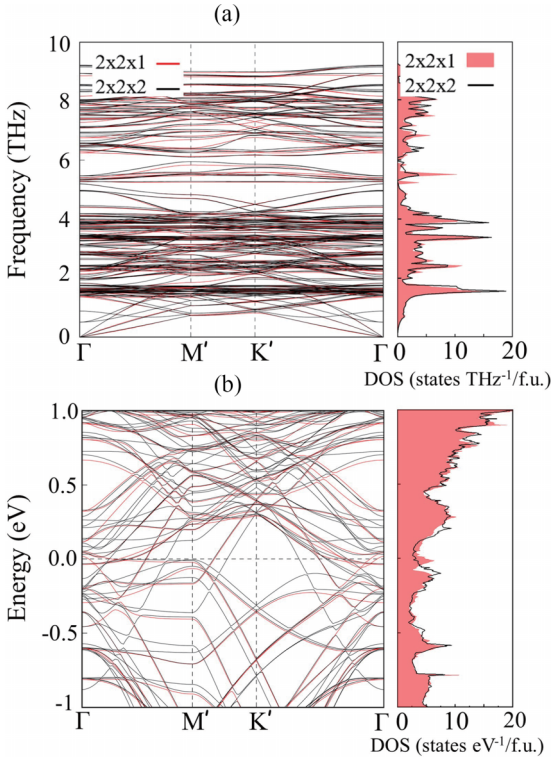

FIG. 2. Calculated (a) phonon spectra and (b) electronic band structures of the 2 × 2 × 1 ISD and 2 × 2 × 2 π-shifted ISD structures, together with the corresponding DOS: see Fig. S2 for the phonon spectrum and electronic band structure of each structure. M′ and K′ represent the M and K points of the 2 × 2 Brillouin zone, respectively.

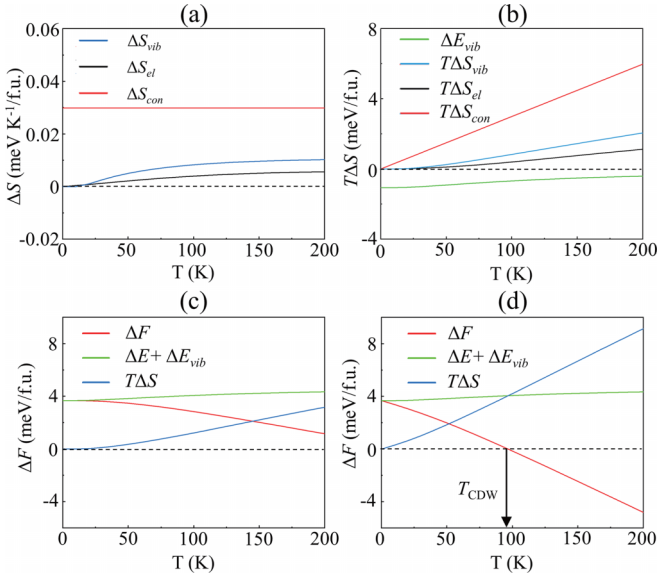

FIG. 3. Calculated (a) $\Delta S_{\rm vib}$, $\Delta S_{\rm el}$, $\Delta S_{\rm con}$, (b) $T\Delta S_{\rm vib}$, $T\Delta S_{\rm el}$, $T\Delta S_{\rm con}$, and $\Delta E_{\rm vib}$ as a function of T. The ΔF vs T curves without and with inclusion of $T\Delta S_{\rm con}$ are plotted in (c) and (d), respectively, where the components of $\Delta E + \Delta E_{\rm vib}$ and $T\Delta S$ are also displayed.

d-ISD constitutes a random stacking of four possible ISD configurations [see Fig. 1(c)] between neighboring kagome layers. It is noted that there are four degenerate 2×2×1 ISD configurations which can be represented by $(\delta_1, \delta_2, \delta_3) = (\delta, \delta, \delta)$, $(\delta,-\delta,-\delta)$, $(-\delta, \delta,-\delta)$, and $(-\delta,-\delta, \delta)$ with $\delta > 0$ [see Fig. 1(c)]. For each 2×2×1 ISD configuration, the V-atom displacements Δd_i of D_i $(i = 1, 2, 3)$ in each unit cell $\mathbf{R}_j$ can be described as $\Delta d_i(\mathbf{R}_j) = \delta_i \cos(\mathbf{Q}_i \cdot \mathbf{R}_j)$. Considering that the disordered phase of AV_3Sb_5 above $T_{\rm CDW}$ was observed to exhibit strong CDW fluctuations [30–32], we treat d-ISD with fast dynamic fluctuations between the four degenerate ISD configurations in each kagome layer, as discussed below. Therefore, the time-averaged structure of d-ISD can be simulated using the 2×2×1 ISD structure with the same stacking of ISD along the c axis. Based on this simulation of d-ISD, we will demonstrate that the thermodynamic feature of the order-disorder CDW phase transition is well captured to properly predict $T_{\rm CDW}$ in RbV_3Sb_5.

The calculated phonon spectra and electronic band structures of the 2×2×1 ISD and 2×2×2 π-shifted ISD structures are displayed in Figs. 2(a) and 2(b), respectively. We find that the latter ISD is more stable than the former ISD by $\Delta E = E_{d-\rm ISD}$ - $E_{\pi-\rm ISD} = 4.75$ meV per formula unit (f.u.). Using phonon dispersion curves, we estimate $E_{\rm vib}$ as

$$E_{\rm vib} = \sum_{\mathbf{q}N} \hbar\omega_{\mathbf{q}N} \left[\frac{1}{2} + \frac{1}{\exp(\hbar\omega_{\mathbf{q}N}/k_{\rm B}T) - 1} \right], \qquad (1)$$

where $\mathbf{q}$ and N represent the wave vector and band index of phonon modes, respectively. $S_{\rm vib}$ is evaluated from the phononic DOS $g_{\rm ph}(\epsilon)$:

$$S_{\rm vib} = -3k_B \int (n_{BE}(\epsilon)\ln[n_{BE}(\epsilon)] - [1 + n_{BE}(\epsilon)]\ln[1 + n_{BE}(\epsilon)])g_{\rm ph}(\epsilon)d\epsilon, \qquad (2)$$

where $n_{BE}(\epsilon)$ is the Bose-Einstein population of a state of energy ϵ at T. Meanwhile, $S_{\rm el}$ is given by

$$S_{\rm el} = -k_B \int (n_{FD}(\epsilon)\ln[n_{FD}(\epsilon)] + [1 - n_{FD}(\epsilon)]\ln[1 - n_{FD}(\epsilon)])g_{\rm el}(\epsilon)d\epsilon, \qquad (3)$$

where $g_{\rm el}(\epsilon)$ is the electronic DOS and $n_{FD}(\epsilon)$ is the Fermi-Dirac distribution function.

Figure 3(a) displays $\Delta S_{\rm vib} = S_{{\rm vib},d-\rm ISD}$ - $S_{{\rm vib},\pi-\rm ISD}$ and $\Delta S_{\rm el} = S_{{\rm el},d-\rm ISD}$ - $S_{{\rm el},\pi-\rm ISD}$ as a function of temperature. We find that d-ISD has larger $S_{\rm vib}$ values than π-ISD, thereby leading to an increase in $T\Delta S_{\rm vib}$ with increasing T [see Fig. 3(b)]. Similarly, d-ISD having a relatively higher $g_{\rm el}(E_F)$ [see Fig. 2(d)] also shows larger $S_{\rm el}$ values than π-ISD. However, due to the smaller magnitude of $\Delta S_{\rm el}$ than $\Delta S_{\rm vib}$, $T\Delta S_{\rm el}$ increases slowly with respect to T [see Fig. 3(b)]. As shown in Fig. 3(b), $\Delta E_{\rm vib} = E_{{\rm vib},d-\rm ISD}$ - $E_{{\rm vib},\pi-\rm ISD}$ is negative, indicating that d-ISD has lower vibrational energy than π-ISD. To manifest the significant role of $S_{\rm con}$ in the order-disorder CDW phase transition, we calculate $\Delta F' = \Delta E + \Delta E_{\rm vib}$ - $T(\Delta S_{\rm vib} + \Delta S_{\rm el})$ without including $T\Delta S_{\rm con}$. As shown in Fig. 3(c), $\Delta F'$ remains positive even up to 200 K, indicating the absence of the order-disorder transition from π-ISD to d-ISD. We will show later that the inclusion of $T\Delta S_{\rm con}$ in ΔF

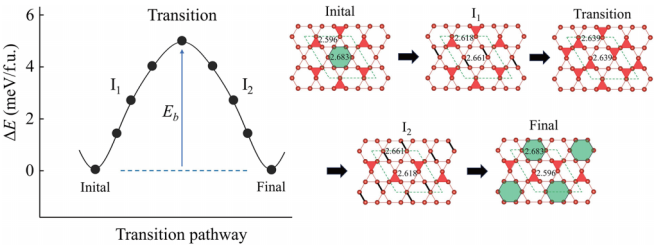

FIG. 4. Calculated energy profile along the transition pathway between two degenerate 2×2×1 ISD configurations. The V kagome geometries of the intial, intermediate I_1 and I_2, transition, and final states are drawn. The numbers represent V-V bond lengths in Å.

is essential for the prediction of an order-disorder CDW phase transition at close to the experimental T_{CDW}.

To unveil the atomic-scale processes of CDW fluctuations above T_{CDW}, we calculate the energy profile along the transition pathway between two degenerate 2×2×1 ISD configurations by using the nudged elastic-band method [47,48]. The calculated energy profile is displayed in Fig. 4, together with the V kagome geometries of the intial, intermediate (I), transition, and final states. We find that the transition state is higher in energy than the initial or final 2×2×1 ISD by 4.98 meV/f.u., yielding an energy barrier $E_b = 4.98$ meV. As shown in Fig. 4, the initial or final state has the V-V bond lengths $d = 2.596$ and 2.683 Å for V trimers and hexamers, respectively. Along the transition pathway, the longer V-V bonds of V hexamers are partially broken in the I_1 state and subsequently new V-trimers are formed in the final state (see Fig. 4). Simultaneously, the bond breaking of V trimers occurs in the I_2 state and finally new V hexamers are formed in the final state. These variations of the V-V bonds indicate that CDW fluctuations occur via the concerted V-V bond breakages and formations of V trimers and hexamers, with a shift of one pristine lattice constant along the $\mathbf{Q}_1$, $\mathbf{Q}_2$, or $\mathbf{Q}_3$ direction [see Fig. 1(c)].

Using the Arrhenius equation [51], we estimate the transition rate $R = \nu \exp(-\frac{E_b}{k_B T})$ between two degenerate 2×2×1 ISD configurations. Here, we adopt the attempt frequency ν with the average frequency (∼6.6 THz) of V-derived phonon modes in the 2×2×1 ISD (see Fig. S1 in the Supplemental Material [52]). With $E_b = 4.98$ meV along the transition pathway (see Fig. 4), we obtain $R = 4.08\times10^{12}$ s^{-1} at 120 K, indicating strong CDW fluctuations with a characteristic lifetime of 0.17 ps [53]. Interestingly, this fluctuating CDW lifetime is comparable with that (0.5 ps) measured by ultrafast spectroscopy in cuprates [55]. Based on the thermally activated dynamic fluctuations among the four degenerate configurations, each containing four formula units, we consider configurational entropy, $S_{con} = k_B \ln(4)/4 = 0.03$ meV K^{-1} per formula unit. This leads to a significant variation in $T\Delta S_{con}$ concerning T, as depicted in Fig. 3(b). As shown in Fig. 3(d), $\Delta F = \Delta E + \Delta E_{vib}$ - $T(\Delta S_{vib} + \Delta S_{el} + \Delta S_{con})$ becomes zero at ∼95 K, with $\Delta E_{vib} = -0.71$ meV/f.u., $T\Delta S_{vib} = 0.81$ meV/f.u., $T\Delta S_{el} = 0.38$ meV/f.u., $T\Delta S_{con} = 2.85$ meV/f.u. Therefore, above a temperature of ∼95 K, d-ISD is thermodynamically more stable than π-ISD. However, below ∼95 K, π-ISD emerges due to the suppression of CDW fluctuations between the four degenerate 2 × 2 ISD charge orders in each kagome layer. It is remarkable that such a theoretically predicted T_{CDW} is close to the experimental value of ∼104 K [56], implying that the thermodynamic quantities of the disordered phase above T_{CDW} would be properly predicted from our simulations of d-ISD. We note that, since the magnitude of $T\Delta S_{con}$ is much larger than those of $T\Delta S_{vib}$ and $T\Delta S_{el}$ [see Fig. 3(b)], the configurational entropy plays a crucial role in inducing the order-disorder CDW phase transition in RbV_3Sb_5 [30].

Recently, DS and IXS experiments [30] for RbV_3Sb_5 and CsV_3Sb_5 observed the existence of an order-disorder CDW phase transition at T_{CDW}, where the high-temperature disorder phase was suppressed and replaced by the long-range 2×2×2 CDW order without phonon softening. Specifically, the analysis of DS and IXS spectra [30] with temperature identified the frozen phonon fluctuations of the 2×2×2 CDW order above T_{CDW}, consistent with strong CDW fluctuations observed by an x-ray diffraction experiment [32]. Furthermore, the specific heat measurements [31,32] of AV_3Sb_5 showed the presence of a sharp peak at T_{CDW}, which represents a first-order phase transition with a release of entropy. These experimental evidences of a first-order, order-disorder CDW phase transition are supported by our prediction of the disorder-induced collapse of long-range CDW order with accompanying an emergence of configurational entropy. According to recent polarization- and temperature-dependent Raman measurements [57] for CsV_3Sb_5, a first-order structural phase transition was also observed to occur at ∼65 K below T_{CDW}. This additional order-disorder transition in CsV_3Sb_5 was interpreted as a stacking order-disorder phase transition due to the stacking fault along the c axis, where a competition between the 2×2×2 and 2×2×4 CDW phases is present below T_{CDW} [30]. However, such a stacking disorder state should be absent in RbV_3Sb_5 which has only the 2×2×2 CDW phase with a π-shifted ISD structure [12,49] [see Fig. 1(d)].

IV. CONCLUSION

Based on first-principles DFT calculations and free energy analysis, we have investigated the nature of the observed order-disorder CDW phase transition in RbV_3Sb_5. It is revealed that above T_{CDW}, the dynamic fluctuations between the four degenerate 2×2 ISD charge orders in each kagome layer occur via the concerted reaction processes involving the V-V bond breakages and formations of V trimers and hexamers. The resultant emergence of configurational entropy plays a crucial role in driving the order-disorder phase transition in RbV_3Sb_5. It is important to note that the observed first-order, order-disorder CDW phase transition is distinct from the second-order, displacive transition scenario based on the FSN-driven Peierls-like electronic instability [11,33–36] and phonon softening [18–22], which reflects a phase transition from the pristine phase. The present results have significant implications for understanding the recently reported order-disorder CDW phase transition in other Kagome metals, such as ScV_6Sn_6 [37–39] and FeGe [40].

ACKNOWLEDGMENTS

This work was supported by the National Natural Science Foundation of China (Grant No. 12104130). Z.Z. acknowledges Innovation Program for Quantum Science and Technology (Grant No. 2021ZD0302800) and Y.J. acknowledges National Natural Science Foundation of China (Grant No. 12074099).

S.Y. and C.W. contributed equally to this work.

[1] L. Ye, M. Kang, J. Liu, F. V. Cube, C. R. Wicker, T. Suzuki, C. Jozwiak, A. Bostwick, E. Rotenberg, D. C. Bell, L. Fu, R. Comin, and J. G. Checkelsky, Massive Dirac fermions in a ferromagnetic kagome metal, Nature (London) **555**, 638 (2018).

[2] Y.-P. Lin and R. M. Nandkishore, Complex charge density waves at Van Hove singularity on hexagonal lattices: Haldane-model phase diagram and potential realization in the kagome metals AV_3Sb_5 (A = K, Rb, Cs), Phys. Rev. B **104**, 045122 (2021).

[3] Z. Lin, C. Wang, P. Wang, S. Yi, L. Li, Q. Zhang, Y. Wang, Z. Wang, H. Huang, Y. Sun *et al.*, Dirac fermions in antiferromagnetic FeSn kagome lattices with combined space inversion and time-reversal symmetry, Phys. Rev. B **102**, 155103 (2020).

[4] S.-Y. Yang, Y. Wang, B. R. Ortiz, D. Liu, J. Gayles, E. Derunova, R. G. Hernandez, L. Smejkal, Y. Chen, S. S. P. Parkin, S. D. Wilson, E. S. Toberer, T. Mcqueen, and M. N. Ali, Giant unconventional anomalous Hall effect in the metallic frustrated magnet candidate, Sci. Adv. **6**, eabb6003 (2020).

[5] F. H. Yu, T. Wu, Z. Y. Wang, B. Lei, W. Z. Zhuo, J. J. Ying, and X. H. Chen, Concurrence of anomalous Hall effect and charge density wave in a superconducting topological kagome metal, Phys. Rev. B **104**, L041103 (2021).

[6] L. Nie, K. Sun, W. Ma, D. Song, L. Zheng, Z. Liang, P. Wu, F. Yu, J. Li, M. Shan *et al.*, Concurrence of anomalous Hall effect and charge density wave in a superconducting topological kagome metal, Nature (London) **604**, 59 (2022).

[7] Z. Jiang, H. Ma, W. Xia, Z. Liu, Q. Xiao, Z. Liu, Y. Yang, J. Ding, Z. Huang, J. Liu *et al.*, Observation of electronic nematicity driven by the three-dimensional charge density wave in kagome lattice KV_3Sb_5, Nano Lett. **23**, 5625 (2023).

[8] B. R. Ortiz, S. M. L. Teicher, Y. Hu, J. L. Zuo, P. M. Sarte, E. C. Schueller, A. M. Milinda Abeykoon, M. J. Krogstad, S. Rosenkranz, R. Osborn, R. Seshadri, L. Balents, J. He, and S. D. Wilson, CsV_3Sb_5: A $\mathbb{Z}_2$ topological kagome metal with a superconducting ground state, Phys. Rev. Lett. **125**, 247002 (2020).

[9] B. R. Ortiz, P. M. Sarte, E. M. Kenney, M. J. Graf, S. M. L. Teicher, R. Seshadri, and S. D. Wilson, Superconductivity in the $\mathbb{Z}_2$ kagome metal KV_3Sb_5, Phys. Rev. Mater. **5**, 034801 (2021).

[10] Q. Yin, Z. Tu, C. Gong, Y. Fu, S. Yan and H. Lei, Superconductivity and normal-state properties of kagome metal RbV_3Sb_5 single crystals, Chin. Phys. Lett. **38**, 037403 (2021).

[11] M. L. Kiesel, C. Platt, and R. Thomale, Unconventional Fermi surface instabilities in the kagome Hubbard model, Phys. Rev. Lett. **110**, 126405 (2013).

[12] Y.-X. Jiang, J.-X. Yin, M. M. Denner, N. Shumiya, B. R. Ortiz, J. He, X. Liu, S. S. Zhang, G. Chang, I. Belopolski *et al.*, Unconventional chiral charge order in kagome superconductor KV_3Sb_5, Nat. Mater. **20**, 1353 (2021).

[13] Z. Liang, X. Hou, F. Zhang, W. Ma, P. Wu, Z. Zhang, F. Yu, J.-J. Ying, K. Jiang, L. Shan, Z. Wang, and X.-H. Chen, Three-dimensional charge density wave and surface-dependent vortex-core states in a kagome superconductor CsV_3Sb_5, Phys. Rev. X **11**, 031026 (2021).

[14] X. Zhou, Y. Li, X. Fan, J. Hao, Y. Dai, Z. Wang, Y. Yao, and H.-H. Wen, Origin of charge density wave in the kagome metal CsV_3Sb_5 as revealed by optical spectroscopy, Phys. Rev. B **104**, L041101 (2021).

[15] Note that certain phonon modes with momentum-dependent coupling to the electronic states can lead to the formation of a CDW. This electron-phonon coupling at different momentum points in the Brillouin zone differs from the traditional $q = 2k_F$ (FSN vector) phonon mode softening observed in Peierls instability.

[16] M. D. Johannes and I. I. Mazin, Fermi surface nesting and the origin of charge density waves in metals, Phys. Rev. B **77**, 165135 (2008).

[17] X. Zhu, J. Guo, J. Zhang, and E. W. Plummer, Misconceptions associated with the origin of charge density waves, Adv. Phys.: X **2**, 622 (2017).

[18] H. Luo, Q. Gao, H. Liu, Y. Gu, D. Wu, C. Yi, J. Jia, S. Wu, X. Luo, Y. Xu, L. Zhao, Q. Wang, H. Mao, G. Liu, Z. Zhu, Y. Shi, K. Jiang, J. Hu, Z. Xu, and X. J. Zhou, Electronic nature of charge density wave and electron-phonon coupling in kagome superconductor KV_3Sb_5, Nat. Commun. **13**, 273 (2022).

[19] S. Cho, H. Ma, W. Xia, Y. Yang, Z. Liu, Z. Huang, Z. Jiang, X. Lu, J. Liu, Z. Liu *et al.*, Emergence of new van Hove singularities in the charge density wave state of a topological kagome metal RbV_3Sb_5, Phys. Rev. Lett. **127**, 236401 (2021).

[20] Z. Wang, S. Ma, Y. Zhang, H. Yang, Z. Zhao, Y. Ou, Y. Zhu, S. Ni, Z. Lu, H. Chen *et al.*, Distinctive momentum dependent charge-density-wave gap observed in CsV_3Sb_5 superconductor with topological Kagome lattice, arXiv:2104.05556.

[21] K. Nakayama, Y. Li, T. Kato, M. Liu, Z. Wang, T. Takahashi, Y. Yao, and T. Sato, Multiple Energy Scales and Anisotropic Energy Gap in the Charge-Density-Wave Phase of Kagome Superconductor CsV_3Sb_5, Phys. Rev. B **104**, L161112 (2021).

[22] G. Liu, X. Ma, K. He, Q. Li, H. Tan, Y. Liu, J. Xu, W. Tang, K. Watanabe, T. Taniguchi, L. Gao, Y. Dai, H.-H. Wen, B. Yan, and X. Xi, Observation of anomalous amplitude modes in the kagome metal CsV_3Sb_5, Nat. Commun. **13**, 3461 (2022).

[23] C. Wang, S. Liu, H. Jeon, and J.-H. Cho, Origin of charge density wave in the layered kagome metal CsV_3Sb_5, Phys. Rev. B **105**, 045135 (2022).

[24] It is noted that the Fermi surface nesting and momentum-dependent electron-phonon coupling are closely related mechanisms that are often discussed in the context of CDW formation. Fermi surface nesting identifies the wave vector at which electronic instabilities are most likely to occur, while the momentum-dependent electron-phonon coupling enables the lattice to respond accordingly, facilitating the formation of a CDW. These mechanisms are inherently interconnected and are

best understood as complementary parts of the CDW formation process [25].

[25] P. Grozić, B. Keran, A. M. Kadigrobov, and D. Radić, Charge stripes in the graphene-based materials, Sci. Rep. **13**, 18931 (2023).

[26] C. Wang, S. Liu, H. Jeon, Y. Jia, and J.-H. Cho, Charge density wave and superconductivity in the kagome metal CsV_3Sb_5 around a pressure-induced quantum critical point, Phys. Rev. Mater. **6**, 094801 (2022).

[27] H. Tan, Y. Liu, Z. Wang, and B. Yan, Charge density waves and electronic properties of superconducting kagome metals, Phys. Rev. Lett. **127**, 046401 (2021).

[28] N. Ratcliff, L. Hallett, B. R. Ortiz, S. D. Wilson, and J. W. Harter, Coherent phonon spectroscopy and interlayer modulation of charge density wave order in the kagome metal CsV_3Sb_5, Phys. Rev. Mater. **5**, L111801 (2021).

[29] H. Li, T. T. Zhang, T. Yilmaz, Y. Y. Pai, C. E. Marvinney, A. Said, Q. W. Yin, C. S. Gong, Z. J. Tu, E. Vescovo, C. S. Nelson, R. G. Moore, S. Murakami, H. C. Lei, H. N. Lee, B. J. Lawrie, and H. Miao, Observation of unconventional charge density wave without acoustic phonon anomaly in kagome superconductors AV_3Sb_5 ($A =$ Rb, Cs), Phys. Rev. X **11**, 031050 (2021).

[30] D. Subires, A. Korshunov, A. H. Said, L. Sánchez, B. R. Ortiz, S. D. Wilson, A. Bosak, and S. Blanco-Canosa, Order-disorder charge density wave instability in the kagome metal $(Cs, Rb)V_3Sb_5$, Nat. Commun. **14**, 1015 (2023).

[31] K. Yang, W. Xia, X. Mi, L. Zhang, Y. Gan, A. Wang, Y. Chai, X. Zhou, X. Yang, Y. Guo, and M. He, Charge fluctuations above T_{CDW} revealed by glass like thermal transport in kagome metals AV_3Sb_5 ($A =$ K, Rb, Cs), Phys. Rev. B **107**, 184506 (2023).

[32] Q. Chen, D. Chen, W. Schnelle, C. Felser, and B. D. Gaulin, Charge density wave order and fluctuations above T_{CDW} and below superconducting T_c in the kagome metal CsV_3Sb_5, Phys. Rev. Lett. **129**, 056401 (2022).

[33] R. E. Peierls, *Quantum Theory of Solids* (Oxford University Press, New York, 1955).

[34] W. Kohn, Image of the Fermi surface in the vibration spectrum of a metal, Phys. Rev. Lett. **2**, 393 (1959).

[35] N. S. Dalal and A. Bussmann-Holder, *Ferro- and Antiferroelectricity* (Springer, Berlin, 2007).

[36] W.-S. Wang, Z.-Z. Li, Y.-Y. Xiang, and Q.-H. Wang, Competing electronic orders on kagome lattices at van Hove filling, Phys. Rev. B **87**, 115135 (2013).

[37] S. Cao, C. Xu, H. Fukui, T. Manjo, Y. Dong, M. Shi, Y. Liu, C. Cao, and Y. Song, Competing charge-density wave instabilities in the kagome metal ScV_6Sn_6, Nat. Commun. **14**, 7671 (2023).

[38] G. Pokharel, B. R. Ortiz, L. Kautzsch, S. J. G. Alvarado, K. Mallayya, G. Wu, E.-A. Kim, J. P. C. Ruff, S. Sarker, and S. D. Wilson, Frustrated charge order and cooperative distortions in ScV_6Sn_6, Phys. Rev. Mater. **7**, 104201 (2023).

[39] S. Liu, C. Wang, S. Yao, Y. Jia, Z. Zhang, and J.-H. Cho, Driving mechanism and dynamic fluctuations of charge density waves in the kagome metal ScV_6Sn_6, Phys. Rev. B **109**, L121103 (2024).

[40] C. Shi, Y. Liu, B. B. Maity, Q. Wang, S. R. Kotla, S. Ramakrishnan, C. Eisele, H. Agarwal, L. Noohinejad, Q. Tao, B. Kang, Z. Lou, X. Yang, Y. Qi, X. Lin, Z. Xu, A. Thamizhavel, G. Cao, S. V. Smaalen, S. Cao *et al.*, Disordered structure for long-range charge density wave order in annealed crystals of magnetic kagome FeGe, arXiv:2308.09034.

[41] G. Kresse and J. Hafner, *Ab initio* molecular dynamics for open-shell transition metals, Phys. Rev. B **48**, 13115 (1993).

[42] G. Kresse and J. Furthmüller, Efficiency of *ab initio* total energy calculations for metals and semiconductors using a plane-wave basis set, Comput. Mater. Sci. **6**, 15 (1996).

[43] P. E. Blöchl, Projector augmented-wave method, Phys. Rev. B **50**, 17953 (1994).

[44] J. P. Perdew, K. Burke, and M. Ernzerhof, Generalized gradient approximation made simple, Phys. Rev. Lett. **77**, 3865 (1996); Generalized gradient approximation made simple [Phys. Rev. Lett. 77, 3865 (1996)], **78**, 1396(E) (1997).

[45] A. Togo, L. Chaput, T. Tadano, and I. Tanaka, Implementation strategies in phonopy and phono3py, J. Phys. Soc. Jpn. **92**, 012001 (2023).

[46] A. Togo and I. Tanaka, First principles phonon calculations in materials science, Scr. Mater. **108**, 1 (2015).

[47] G. Henkelman, B. P. Uberuaga, and H. Jónsson, A climbing image nudged elastic band method for finding saddle points and minimum energy paths, J. Chem. Phys. **113**, 9901 (2000).

[48] D. Sheppard, P. Xiao, W. Chemelewski, D. D. Johnson, and G. Henkelman, A generalized solid-state nudged elastic band method, J. Chem. Phys. **136**, 074103 (2012).

[49] M. Kang, S. Fang, J. Yoo, B. R. Ortiz, Y. M. Oey, J. Choi, S. H. Ryu, J. Kim, C. Jozwiak, A. Bostwick, E. Rotenberg, E. Kaxiras, J. G. Checkelsky, S. D. Wilson, J.-H. Park, and R. Comin, Charge order landscape and competition with superconductivity in kagome metals, Nat. Mater. **22**, 186 (2023).

[50] B. R. Ortiz, S. M. L. Teicher, L. Kautzsch, P. M. Sarte, N. Ratcliff, J. Harter, J. P. C. Ruff, R. Seshadri, and S. D. Wilson, Fermi surface mapping and the nature of charge-density-wave order in the kagome superconductor CsV_3Sb_5, Phys. Rev. X **11**, 041030 (2021).

[51] S. Arrhenius, Über die Reaktionsgeschwindigkeit bei der Inversion von Rohrzucker durch Säuren, Z. Phys. Chem. **4U**, 226 (1889).

[52] See Supplemental Material at http://link.aps.org/supplemental/10.1103/PhysRevMaterials.8.064002 for the estimation of the average frequency of V-derived phonon modes in the $2 \times 2 \times 1$ ISD structure and the plots of the phonon spectra and electronic band structures of the $2 \times 2 \times 1$ ISD and $2 \times 2 \times 2\pi$-shifted ISD structures.

[53] The characteristic lifetime (half lifetime) of the transition between two degenerate $2\times2\times1$ ISD configurations is calculated using the equation $t_{1/2} = \ln(2)/R$ [54].

[54] J. I. Steinfeld, J. S. Francisco, and W. L. Hase, *Chemical Kinetics and Dynamics*, 2nd ed. (Prentice Hall, New Jersey, 1999).

[55] D. H. Torchinsky, F. Mahmood, A. T. Bollinger, I. Bozovic, and N. Gedik, Fluctuating charge-density waves in a cuprate superconductor, Nat. Mater. **12**, 387 (2013).

[56] B. R. Ortiz, L. C. Gomes, J. R. Morey, M. Winiarski, M. Bordelon, J. S. Mangum, I. W. H. Oswald, J. A. Rodriguez-Rivera, J. R. Neilson, S. D. Wilson, E. Ertekin, T. M. McQueen, and E. S. Toberer, New kagome prototype materials: Discovery of KV_3Sb_5, RbV_3Sb_5, and CsV_3Sb_5, Phys. Rev. Mater. **3**, 094407 (2019).

[57] F. Jin, W. Ren, M. Tan, M. Xie, B. Lu, Z. Zhang, J. Ji, and Q. Zhang, π Phase interlayer shift and stacking fault in the kagome superconductor CsV_3Sb_5, Phys. Rev. Lett. **132**, 066501 (2024).